INTERNATIONAL JOURNAL OF
NUMERICAL ANALYSIS AND MODELING
Volume 11, Number 1, Pages 172–192

GLOBAL CONVERGENCE OF *A POSTERIORI* ERROR ESTIMATES FOR THE DISCONTINUOUS GALERKIN METHOD FOR ONE-DIMENSIONAL LINEAR HYPERBOLIC PROBLEMS

MAHBOUB BACCOUCH

Abstract. In this paper we study the global convergence of the implicit residual-based *a posteriori* error estimates for a discontinuous Galerkin method applied to one-dimensional linear hyperbolic problems. We apply a new optimal superconvergence result [Y. Yang and C.-W. Shu, *SIAM J. Numer. Anal.*, 50 (2012), pp. 3110-3133] to prove that, for smooth solutions, these error estimates at a fixed time converge to the true spatial errors in the L^2-norm under mesh refinement. The order of convergence is proved to be $k+2$, when k-degree piecewise polynomials with $k \geq 1$ are used. As a consequence, we prove that the DG method combined with the *a posteriori* error estimation procedure yields both accurate error estimates and $\mathcal{O}(h^{k+2})$ superconvergent solutions. We perform numerical experiments to demonstrate that the rate of convergence is optimal. We further prove that the global effectivity indices in the L^2-norm converge to unity under mesh refinement. The order of convergence is proved to be 1. These results improve upon our previously published work in which the order of convergence for the *a posteriori* error estimates and the global effectivity index are proved to be $k+3/2$ and $1/2$, respectively. Our proofs are valid for arbitrary regular meshes using P^k polynomials with $k \geq 1$ and for both the periodic boundary condition and the initial-boundary value problem. Several numerical simulations are performed to validate the theory.

Key words. Discontinuous Galerkin method; hyperbolic problems; superconvergence; residual-based *a posteriori* error estimates.

1. Introduction

In this paper we analyze a residual-based *a posteriori* error estimates of the spatial errors for the semi-discrete discontinuous Galerkin (DG) method applied to the following one-dimensional linear hyperbolic conservation laws

$$u_t + cu_x = f(x,t), \quad x \in [a,b],\ t \in [0,T],\ c > 0, \tag{1.1a}$$

subject to the initial condition

$$u(x,0) = u_0(x), \quad x \in [a,b], \tag{1.1b}$$

and to either the Dirichlet boundary condition

$$u(a,t) = g(t), \quad t \in [0,T], \tag{1.1c}$$

or to the periodic boundary condition

$$u(a,t) = u(b,t), \quad t \in [0,T]. \tag{1.1d}$$

Here $c > 0$ is a constant speed and $[0,T]$ is a finite time interval. In this paper, we consider, without loss of generality, (1.1) with $c = 1$. In our analysis we select

Received by the editors April 7, 2013 and, in revised form, June 8, 2013.
2000 *Mathematics Subject Classification.* 65M60.
This research was partially supported by the NASA Nebraska Space Grant Program and U-CRCA at the University of Nebraska at Omaha.

the initial and boundary conditions and the source, $f(x,t)$, such that the exact solution, $u(x,t)$, is a smooth function on $[a,b]\times[0,T]$.

The DG method considered here is a class of finite element methods using completely discontinuous piecewise polynomials for the numerical solution and the test functions. DG method combines many attractive features of the classical finite element and finite volume methods. It is a powerful tool for approximating some partial differential equations which model problems in physics, especially in fluid dynamics or electrodynamics. In particular, it provides an appealing approach to address problems having discontinuities, such as those that arise in hyperbolic conservation laws. DG method was initially introduced by Reed and Hill in 1973 as a technique to solve neutron transport problems [30]. In 1974, LaSaint and Raviart [29] presented the first numerical analysis of the method for a linear advection equation. Since then, DG methods have been used to solve ordinary differential equations [5, 18, 28, 29], hyperbolic [14, 15, 16, 17, 23, 24, 26, 27] and diffusion and convection-diffusion [12, 13, 31] partial differential equations. Consult [22] and the references cited therein for a detailed discussion of the history of DG method and a list of important citations on the DG method and its applications.

In recent years, the study of superconvergence and *a posteriori error* estimates of DG methods has been an active research field in numerical analysis. *A posteriori* error estimators employ the known numerical solution to derive estimates of the actual solution errors. They are also used to steer adaptive schemes where either the mesh is locally refined (h-refinement) or the polynomial degree is raised (p-refinement). For an introduction to the subject of *a posteriori* error estimation see the monograph of Ainsworth and Oden [9]. A knowledge of superconvergence properties can be used to (i) construct simple and asymptotically exact *a posteriori* estimates of discretization errors like the one considered in this paper and (ii) help detect discontinuities to find elements needing limiting, stabilization and/or refinement. Superconvergence properties for DG methods have been studied in [5, 8, 25, 29] for ordinary differential equations, [4, 10, 5, 7, 21, 32] for hyperbolic problems and [2, 3, 6, 7, 11, 19, 20, 21] for diffusion and convection-diffusion problems.

The first superconvergence result for standard DG solutions of ordinary differential equations appeared in Adjerid *et al.* [5]. They proved that the k-degree DG solution of $u'-au=0$ is $\mathcal{O}(h^{k+2})$ superconvergent at the roots of $(k+1)$-degree right Radau polynomial. Numerical computations indicate that these superconvergence results extend to DG solutions of transient convection problems. However no analysis has been carried out for these results. Later, Cheng and Shu [21] studied the superconvergence property for the DG methods for solving one-dimensional time-dependent linear conservation laws. They proved superconvergence towards a particular projection of the exact solution when the upwind flux is used. The order of superconvergence is proved to be $k+3/2$, when k-degree piecewise polynomials with $k\geq 1$ are used. However, the superconvergence rate obtained in [21] is not optimal. Adjerid and Baccouch [4] investigated the global convergence of the implicit residual-based *a posteriori* error estimates of Adjerid *et al.* [5]. They applied the superconvergence results of Cheng and Shu [21] and proved that these estimates at a fixed time t converge to the true spatial error in the L^2-norm under mesh refinement. The order of superconvergence is proved to be $k+3/2$. They further proved that the global effectivity indices converge to unity at $\mathcal{O}(h^{1/2})$ rate. In this paper, we improve upon the result in [4]. A new optimal superconvergence

result is used to obtain optimal convergence rate in the L^2-norm for the *a posteriori* error estimates and higher convergence rate for the global effectivity index.

More recently, Y. Yang and C.-W. Shu [32] studied the superconvergence of the error for the DG method for linear conservation laws. They proved that the error between the k-degree DG solution and the exact solution is $(k+2)^{th}$ order superconvergent at the downwind-biased Radau points with suitable initial discretization. They further proved that the DG solution is $(k+2)^{th}$ order superconvergent both for the cell averages and for the error to a particular projection of the exact solution. Their analysis is valid for arbitrary regular meshes and for P^k polynomials with arbitrary $k \geq 1$, and for both periodic boundary conditions and for initial-boundary value problems. They performed numerical experiments to demonstrate that the superconvergence rate is optimal.

In this paper, we study the global convergence of the implicit residual-based *a posteriori* error estimates for scalar linear hyperbolic problems. We apply the new optimal superconvergence result [32] to prove that these estimates at a fixed time t converge to the true spatial errors in the L^2-norm under mesh refinement. The order of convergence is proved to be $k+2$. As a consequence, we prove that the DG method combined with the *a posteriori* error estimation procedure yields both accurate error estimates and $\mathcal{O}(h^{k+2})$ superconvergent solutions. Numerical evidences suggest that the rate of convergence is optimal. We further prove that the global effectivity indices converge to unity under mesh refinement. The order of convergence is proved to be 1. These results improve upon our previously published work [4] in which the order of convergence in the L^2-norm for the *a posteriori* error estimates and the global effectivity index are proved to be $k+3/2$ and $1/2$, respectively. Even though our proofs are given for a simple initial-boundary value problem, the same results can be easily obtained for one-dimensional linear systems along the same lines. Furthermore, our proofs are valid for any regular meshes any using piecewise polynomials of degree $k \geq 1$ and for both the periodic boundary condition and the initial-boundary value problem. Several numerical simulations are performed to validate the theory.

This paper is organized as follows: In section 2 we present the semi-discrete DG method for solving the one-dimensional linear hyperbolic problem and recall some superconvergence results needed for our analysis. In section 3, we present our *a posteriori* error estimation procedure and prove that these error estimates converge to the true errors under mesh refinement in L^2-norm. In section 4, we present several numerical examples to demonstrate the asymptotic exactness of the *a posteriori* error estimates under mesh refinement in L^2-norm. We conclude and discuss our results in section 5.

2. The DG method for conservation laws

In order to obtain the semi-discrete DG method, we divide $I=[a,b]$ into N subintervals $I_i=[x_{i-1},x_i],\ i=1,\ldots,N$, where $a=x_0<\cdots<x_N=b$. Throughout this paper, the length I_i is denoted by $h_i=x_i-x_{i-1}$. We denote $h=\max\limits_{1\leq i\leq N} h_i$ and $h_{min}=\min\limits_{1\leq i\leq N} h_i$ as the length of the largest and smallest subinterval. Here, we consider regular meshes, that is $h\leq Kh_{min}$, where $K\geq 1$ is a constant during mesh refinement. If $K=1$, then the mesh is uniformly distributed. Throughout

this paper, $v\big|_i$, $v^-\big|_i$, and $v^+\big|_i$, respectively, denote the value, the left limit, and the right limit of the function v at x_i, *i.e.*,

$$v\big|_i = v(x_i,t), v^-\big|_i = v^-(x_i,t) = \lim_{s\to 0^-} v(x_i+s,t), v^+\big|_i = v^+(x_i,t) = \lim_{s\to 0^+} v(x_i+s,t).$$

In order to obtain the weak DG formulation, we multiply (1.1a) by a test function v, integrate over an arbitrary element I_i, and use integration by parts to write

$$\int_{I_i} u_t v \, dx - \int_{I_i} uv_x \, dx + uv\big|_i - uv\big|_{i-1} = \int_{I_i} fv \, dx. \tag{2.1}$$

We construct a finite dimensional space V_h^k of discontinuous piecewise polynomials such that

$$V_h^k = \{v : \ v|_{I_i} \in P^k(I_i), \text{ for } x \in I_i, \ i = 1, \ldots, N\},$$

where $P^k(I_i)$ is the space of polynomials of degree at most k on I_i. Note that polynomials in the space V_h^k are allowed to have discontinuities across element boundaries.

The semi-discrete DG method consists of finding $u_h(.,t) \in V_h^k$ such that: $\forall\ i = 1, \cdots, N$,

$$\int_{I_i} (u_h)_t v \, dx - \int_{I_i} u_h v_x \, dx + \tilde{u}_h v^-\big|_i - \tilde{u}_h v^+\big|_{i-1} = \int_{I_i} fv \, dx, \quad \forall\ v \in V_h^k, \tag{2.2a}$$

where $\tilde{u}_h\big|_i$ is the so-called numerical flux, which is yet to be determined. This numerical flux is nothing but discrete approximation to the trace of u at $x = x_i$. It must be designed to ensure the stability and accuracy of the scheme. In order to complete the definition of the DG method we need to select the numerical flux $\tilde{u}_h$ on the boundaries of I_i. For the boundary condition (1.1c), the numerical flux associated with the convection is taken as the classical upwind flux *i.e.*,

$$\tilde{u}_h\big|_0 = g(t), \quad \text{and} \quad \tilde{u}_h\big|_i = u_h^-\big|_i, \ i = 1, \ldots, N. \tag{2.2b}$$

If the periodic boundary condition (1.1d) is chosen, the numerical flux $\tilde{u}_h$ can be taken as

$$\tilde{u}_h\big|_0 = u_h^-\big|_N, \quad \text{and} \quad \tilde{u}_h\big|_i = u_h^-\big|_i, \ i = 1, \ldots, N.$$

The initial condition $u_h(x,0) \in V_h^k$ is obtained using a special projection of the exact initial condition $u(x,0)$. This particular projection will be defined later.

Expressing $u_h(x,t) = \sum_{j=0}^k c_j(t)\phi_j(x), \ x \in I_i$ as a linear combination of orthogonal basis $\phi_j(x), \ j = 0, \ldots, k$ (in our numerical examples ϕ_j is the j^{th}-degree Legendre polynomial on I_i), and testing against functions $v = \phi_j, \ j = 0, \ldots, k$, we obtain a system of ordinary differential equations which can be solved for the coefficients c_j. In practice, the system is solved using *e.g.*, the classical fourth-order Runge-Kutta method. A time step is chosen so that temporal errors are small relative to spatial errors.

Notations, definitions, and preliminary results. For $k \geq 1$, we will consider a special projection operator, P_h^-, which is defined as follows: For any smooth function u, the restriction of $P_h^- u$ to I_i is defined as the unique element of $P^k(I_i)$ satisfying

$$\int_{I_i} (P_h^- u - u) v dx = 0, \ \forall\ v \in P^{k-1}(I_i), \quad \text{and} \quad (P_h^- u)^-\big|_i = u^-\big|_i. \tag{2.3}$$

This special projection is used in the error estimates of the DG methods to derive optimal L^2 error bounds in the literature; see *e.g.*, [21].

In this paper, we define the L^2 inner product of two integrable functions, $u = u(x,t)$ and $v = v(x,t)$, depending on x and t on the interval $I_i = [x_{i-1}, x_i]$ as

$$(u(.,t), v(.,t))_{0,I_i} = \int_{I_i} u(x,t)v(x,t)dx. \tag{2.4a}$$

Denote $\|u(.,t)\|_{0,I_i} = ((u(.,t), u(.,t))_{0,I_i})^{1/2}$ to be the standard L^2-norm of u on I_i. For convenience, we use $\|u(.,t)\|_{I_i}$ to denote $\|u(.,t)\|_{0,I_i}$.

Let $H^s(I_i)$, where $s = 1, 2, \ldots$, denote the standard Sobolev space of square integrable functions on I_i with all derivatives $\frac{\partial^j u}{\partial x^j}$, $j = 1, 2, \ldots, s$ being square integrable on I_i and equipped with the norm

$$\|u(.,t)\|_{s,I_i} = \left(\sum_{j=0}^{s} \left\| \frac{\partial^j u(.,t)}{\partial x^j} \right\|_{I_i}^2 \right)^{1/2}.$$

We also define the norms on the whole computational domain I as follows:

$$\|u(.,t)\|_I = \left(\sum_{i=1}^{N} \|u(.,t)\|_{I_i}^2 \right)^{1/2}, \quad \|u(.,t)\|_{s,I} = \left(\sum_{i=1}^{N} \|u(.,t)\|_{s,I_i}^2 \right)^{1/2}.$$

We note that if $u \in H^s(I)$, $s = 1, 2, \ldots$, the norms $\|u(.,t)\|_{s,I}$ on the whole computational domain is the standard Sobolev norm $\left(\sum_{j=0}^{s} \left\| \frac{\partial^j u(.,t)}{\partial x^j} \right\|_I^2 \right)^{1/2}$.

For convenience, we use $\|u\|$ to denote $\|u\|_I$. Also, in the remainder of this paper, we will omit the notation $(.,t)$ used in the subsequent induced norms unless needed for clarity. Thus we use $\|u\|_{s,I_i}$ instead of $\|u(.,t)\|_{s,I_i}$ etc.

In our analysis we need the k^{th}-degree Legendre polynomial defined by Rodrigues formula [1]

$$\tilde{L}_k(\xi) = \frac{1}{2^k k!} \frac{d^k}{d\xi^k}[(\xi^2 - 1)^k], \quad -1 \le \xi \le 1,$$

which satisfies the following properties: $\tilde{L}_k(1) = 1$, $\tilde{L}_k(-1) = (-1)^k$ and the orthogonality relation

$$\int_{-1}^{1} \tilde{L}_k(\xi)\tilde{L}_p(\xi)d\xi = \frac{2}{2k+1}\delta_{kp}, \quad \text{where } \delta_{kp} \text{ is the Kronecker symbol.} \tag{2.5}$$

The $(k+1)$-degree Legendre polynomial on $[-1, 1]$ can be written as

$$\tilde{L}_{k+1}(\xi) = \frac{(2k+2)!}{2^{k+1}[(k+1)!]^2}\xi^{k+1} + \tilde{q}_k(\xi), \quad \text{where } \tilde{q}_k \in P^k.$$

Next, we define the $(k+1)-$degree right Radau polynomial as

$$\tilde{R}_{k+1}(\xi) = \tilde{L}_{k+1}(\xi) - \tilde{L}_k(\xi), \ -1 \le \xi \le 1, \tag{2.6a}$$

which has $k+1$ real distinct roots, $-1 < \xi_0 < \cdots < \xi_k = 1$.

Mapping the element $I_i = [x_{i-1}, x_i]$ into a reference element $[-1, 1]$ by the standard affine mapping

$$x(\xi, h_i) = \frac{x_i + x_{i-1}}{2} + \frac{h_i}{2}\xi, \tag{2.6b}$$

we obtain the shifted right Radau polynomial on I_i

$$R_{k+1,i}(x) = \tilde{R}_{k+1}\left(\frac{2x - x_i - x_{i-1}}{h_i}\right) = \frac{(2k+2)!}{h_i^{k+1}[(k+1)!]^2}x^{k+1} + r_k(x), \quad \text{where } r_k \in P^k.$$

Next, we define the monic right Radau polynomial, $\psi_{k+1,i}(x)$, on I_i as

$$\psi_{k+1,i}(x) = \frac{[(k+1)!]^2}{(2k+2)!}h_i^{k+1}R_{k+1,i}(x) = c_k h_i^{k+1}R_{k+1,i}(x) = \prod_{j=0}^{k}(x - x_{i,j}), \tag{2.6c}$$

where $c_k = \frac{[(k+1)!]^2}{(2k+2)!}$ and $x_{i,j} = \frac{x_i + x_{i-1}}{2} + \frac{h_i}{2}\xi_j,\ j = 0, 1, \ldots, k$, are the roots of $R_{k+1,i}(x)$ shifted to I_i.

Next we state and prove the following result which will be needed in our *a posteriori* error analysis.

Lemma 2.1. *The $(k+1)$-degree monic Radau polynomial on I_i, $\psi_{k+1,i}(x)$, satisfies*

$$(\psi'_{k+1,i}, \psi_{k+1,i})_{I_i} = -2c_k^2 h_i^{2k+2}, \tag{2.7a}$$

$$\|\psi_{k+1,i}\|^2_{I_i} = d_k h_i^{2k+3}, \tag{2.7b}$$

where

$$c_k = \frac{[(k+1)!]^2}{(2k+2)!}, \quad d_k = \frac{2(2k+2)}{(2k+1)(2k+3)}c_k^2. \tag{2.7c}$$

Proof. Since $\tilde{L}_k(1) = 1$ and $\tilde{L}_k(-1) = (-1)^k$, we have $\tilde{R}_{k+1}(1) = R_{k+1}(x_i) = \psi_{k+1,i}(x_i) = 0$ and $\tilde{R}_{k+1}(-1) = R_{k+1}(x_{i-1}) = 2(-1)^{k+1}$. Thus,

$$\begin{aligned}
&(\psi'_{k+1,i}, \psi_{k+1,i})_{I_i} \\
= &\int_{I_i} \psi'_{k+1,i}(x)\psi_{k+1,i}(x)dx = \frac{1}{2}\psi^2_{k+1,i}(x_i) - \frac{1}{2}\psi^2_{k+1,i}(x_{i-1}) = -\frac{1}{2}\psi^2_{k+1,i}(x_{i-1}) \\
= &-\frac{1}{2}\left[c_k h_i^{k+1}R_{k+1,i}(x_{i-1})\right]^2 = -\frac{1}{2}\left[c_k h_i^{k+1}\tilde{R}_{k+1}(-1)\right]^2 = -2c_k^2 h_i^{2k+2}.
\end{aligned}$$

Next, we will prove (2.7b). Using (2.6b) and the orthogonality relation (2.5), we have

$$\begin{aligned}
&\|\psi_{k+1,i}\|^2_{I_i} \\
= &\int_{I_i} \psi^2_{k+1,i}(x)dx = c_k^2 h_i^{2k+2}\int_{I_i} R^2_{k+1}(x)dx = c_k^2 h_i^{2k+2}\frac{h_i}{2}\int_{-1}^{1}\tilde{R}^2_{k+1}(\xi)d\xi \\
= &\frac{c_k^2 h_i^{2k+3}}{2}\int_{-1}^{1}\left(\tilde{L}_{k+1}(\xi) - \tilde{L}_k(\xi)\right)^2 d\xi = \frac{c_k^2 h_i^{2k+3}}{2}\int_{-1}^{1}(\tilde{L}^2_{k+1}(\xi) + \tilde{L}^2_k(\xi))d\xi \\
= &\frac{c_k^2 h_i^{2k+3}}{2}\left[\frac{2}{2k+3} + \frac{2}{2k+1}\right] = \frac{2(2k+2)}{(2k+1)(2k+3)}c_k^2 h_i^{2k+3} = d_k h_i^{2k+3},
\end{aligned}$$

where $d_k = \frac{2(2k+2)}{(2k+1)(2k+3)}c_k^2$. □

Next, we consider an interpolation operator π which is defined as follows: For any function $u = u(x,t)$ with $t \in [0,T]$ kept fixed, $\pi u\big|_{I_i} \in P^k(I_i)$ and interpolates u at the roots $x_{i,j},\ j = 0, 1, \ldots, k$, of $(k+1)$-degree right Radau polynomial shifted to I_i.

For the sake of completeness, we include the following results from [4] which will be needed in our error analysis.

Lemma 2.2. *Let $u \in H^{k+2}$, $t \in [0,T]$ fixed, and P_h^- and π as defined above. Then*

$$u - \pi u = \phi_i + \gamma_i, \ \ on \ \ I_i, \tag{2.8a}$$

where

$$\phi_i(x,t) = \alpha_i(t)\psi_{k+1,i}(x), \quad \psi_{k+1,i}(x) = \prod_{j=0}^{k}(x - x_{i,j}), \tag{2.8b}$$

$$\|\phi_i\|_{s,I_i} \leq C h_i^{k+1-s} \ \|u\|_{k+1,I_i}, \quad s = 0, \cdots, k, \tag{2.8c}$$

$$\|\gamma_i\|_{s,I_i} \leq C h_i^{k+2-s} \ \|u\|_{k+2,I_i}, \quad s = 0, \cdots, k+1. \tag{2.8d}$$

Moreover,

$$\left\|\pi u - P_h^- u\right\|_{I_i} \leq C h_i^{k+2} \ \|u\|_{k+2,I_i}. \tag{2.9}$$

Proof. The proof of these results can be found in the paper by Adjerid and Baccouch [4]. □

Throughout this paper, we use e, ϵ, and $\bar{e}$ to denote, respectively, the error between the exact solution of (1.1) and the numerical solution defined in (2.2), the projection error, and the error between the numerical solution and the projection of the exact solution, *i.e.*,

$$e = u - u_h, \qquad \epsilon = u - P_h^- u, \qquad \bar{e} = P_h^- u - u_h.$$

We note that the true error can be split as $e = \epsilon + \bar{e}$.

In [32], the authors analyzed the same semi-discrete DG method considered here. They selected a special projection of the initial condition $u_h(x,0) \in V_h^k$ and proved that the DG solution is $\mathcal{O}(h^{k+2})$ super close to $P_h^- u$. This special projection is designed to better control the error of the initial condition. In particular, in their analysis, they designed the initial condition $u_h(x,0)$ so that the following two requirements hold: (i) $\bar{e}_t(x,0) = 0$ and (ii) $\|\bar{e}(x,0)\| = \mathcal{O}(h^{k+2})$. See [32] for the exact implementation of the initial discretization.

For the sake of completeness, we summarize their results in the next theorem [32].

Theorem 2.1. *Let u be the exact solution of (1.1). If $k \geq 1$ and u_h is the DG solution defined in (2.2), then there exist positive constants C_1, C_2, C_3 independent of h such that $\forall\ t \in [0,T]$*

$$\|\bar{e}\| \ \leq \ C_1 h^{k+2}. \tag{2.10a}$$

$$\|e\| \ \leq \ C_2 h^{k+1}. \tag{2.10b}$$

$$\|e_t\| \ \leq \ C_3 h^{k+1}. \tag{2.10c}$$

Here $C_1 = \hat{C}_1(T+1)\|u\|_{k+4,I}$, $C_2 = \hat{C}_2(T+1)\|u\|_{k+3,I}$, $C_3 = \hat{C}_3(T+1)\|u\|_{k+3,I}$, and the constants $\hat{C}_j$, $j = 1,2,3$ are independent of h, T, and u.

Proof. These results have been proved in [32]. More precisely, the estimate (2.10a) can be found in its Corollary 2.1. The results (2.10b) and (2.10c) can be found in the proof of the main result of its Theorem 2.1 (page 3118). □

From now on, the notation $C,\ C_1,\ C_2$, etc. will be used to denote positive constants that are independent of the discretization parameter h, but which may depend upon the exact solution u. Furthermore, all the constants will be generic, *i.e.*, they may represent different constant quantities in different occurrences.

In the next theorem, we state and prove the following superconvergence result.

Theorem 2.2. *Under the assumptions of Theorem 2.1, then there exists a positive constant C independent of h such that*

$$\|u_h - \pi u\| \leq Ch^{k+2}. \tag{2.11}$$

Moreover, the true error can be divided into a significant part and a less significant part as

$$e(x,t) = \alpha_i(t)\psi_{k+1,i}(x) + \omega_i(x,t), \ \ on \ \ \ I_i, \tag{2.12a}$$

where

$$\omega_i = \gamma_i + \pi u - u_h, \tag{2.12b}$$

and

$$\sum_{i=1}^{N} \|\omega_i\|_{I_i}^2 \leq Ch^{2(k+2)}, \qquad \sum_{i=1}^{N} \|(\omega_i)_x\|_{I_i}^2 \leq Ch^{2(k+1)}. \tag{2.12c}$$

Finally,

$$\sum_{i=1}^{N} \|e_x\|_{I_i}^2 \leq Ch^{2k} \quad \textit{and} \quad \|e\|_{1,I} \leq Ch^k. \tag{2.13}$$

Proof. Adding and subtracting $P_h^- u$ to $u_h - \pi u$, we write

$$u_h - \pi u = u_h - P_h^- u + P_h^- u - \pi u = -\bar{e} + P_h^- u - \pi u.$$

Taking the L^2-norm and applying the triangle inequality, we obtain

$$\|u_h - \pi u\| \leq \|\bar{e}\| + \left\|P_h^- u - \pi u\right\|.$$

Using the estimates (2.10a) and (2.9) we establish (2.11).

Next, we add and subtract πu to e, we have

$$e = u - \pi u + \pi u - u_h. \tag{2.14}$$

Furthermore, one can split the interpolation errors $u - \pi u$ on $\ I_i$ as in (2.8a) to obtain

$$e = \phi_i + \gamma_i + \pi u - u_h = \phi_i + \omega_i, \quad \text{where} \quad \omega_i = \gamma_i + \pi u - u_h. \tag{2.15}$$

Next, we use Cauchy-Schwarz inequality and the inequality $|ab| \leq \frac{1}{2}(a^2 + b^2)$ to write

$$\begin{aligned} \|\omega_i\|_{I_i}^2 &= (\gamma_i + \pi u - u_h, \gamma_i + \pi u - u_h)_{I_i} = \|\gamma_i\|_{I_i}^2 + 2\,(\gamma_i, \pi u - u)_{I_i} + \|\pi u - u_h\|_{I_i}^2 \\ &\leq 2\left(\|\gamma_i\|_{I_i}^2 + \|\pi u - u_h\|_{I_i}^2\right). \end{aligned} \tag{2.16}$$

Summing over all elements and applying (2.8d) with $s = 0$ and (2.11) yields the first estimate in (2.12c).

Next we will prove the second estimate in (2.12c). Using Cauchy-Schwarz inequality and the inequality $|ab| \leq \frac{1}{2}(a^2+b^2)$, we write

(2.17)
$$\|(\omega_i)_x\|^2_{I_i} = ((\gamma_i)_x + (\pi u - u_h)_x, (\gamma_i)_x + (\pi u - u_h)_x)_{I_i} \leq 2\left(\|(\gamma_i)_x\|^2_{I_i} + \|(\pi u - u_h)_x\|^2_{I_i}\right).$$

Using the inverse inequality $\|(\pi u - u_h)_x\|_{I_i} \leq C\ h^{-1}\|(\pi u - u_h)\|_{I_i}$, we obtain the estimate

$$\|(\omega_i)_x\|^2_{I_i} \leq C\left(\|(\gamma_i)_x\|^2_{I_i} + h^{-2}\|\pi u - u_h\|^2_{I_i}\right).$$

Summing over all elements and applying (2.11) and the standard error estimates (2.8d) with $s=1$ we establish the second estimate in (2.12c).

In order to show (2.13), we note that

$$\|e\|^2_{1,I} = \|e\|^2 + \sum_{i=1}^{N}\|e_x\|^2_{I_i}. \tag{2.18}$$

Differentiating (2.15) with respect to x, taking the L^2-norm, and applying Cauchy-Schwarz inequality and the inequality $|ab| \leq \frac{1}{2}(a^2+b^2)$, we get

$$\|e_x\|^2_{I_i} \quad = \quad ((\phi_i)_x + (\omega_i)_x, (\phi_i)_x + (\omega_i)_x)_{I_i} \leq 2\left(\|(\phi_i)_x\|^2_{I_i} + \|(\omega_i)_x\|^2_{I_i}\right).$$

Summing over all elements and applying (2.8c) and (2.12c), we obtain

$$\sum_{i=1}^{N}\|e_x\|^2_{I_i} \leq Ch^{2k}. \tag{2.19}$$

Finally, substituting (2.10b) and (2.19) into (2.18) establishes (2.13). □

The results of the previous theorem show that the k-degree DG solution is $\mathcal{O}(h^{k+2})$ superconvergent at the roots of $(k+1)$-degree right Radau polynomial. This proves the observed numerical results in [5]. This error analysis allows us to obtain optimal convergence rate for the *a posteriori* error estimates [4] to the true spatial errors in the L^2-norm under mesh refinement.

3. *A posteriori* error estimation

We first present the weak finite element formulation to compute the *a posteriori* error estimate for the scalar hyperbolic equation [5]. Replacing u by u_h+e, equation (1.1) yields

$$e_x + e_t = r_h, \tag{3.1a}$$

where the residual is given by

$$r_h = f - (u_h)_t - (u_h)_x. \tag{3.1b}$$

Multiplying (3.1a) by arbitrary smooth test function v and integrating over an arbitrary element I_i, we obtain

$$(e_x, v)_{I_i} \quad = \quad (r_h - e_t, v)_{I_i}. \tag{3.2}$$

Substituting (2.12a) into the left-hand sides of (3.2) and choosing $v = \psi_{k+1,i}(x)$ we obtain

$$\alpha_i(\psi'_{k+1,i}, \psi_{k+1,i})_{I_i} = (r_h - e_t - (\omega_i)_x, \psi_{k+1,i})_{I_i}. \tag{3.3a}$$

Using the property (2.7a) and solving (3.3a) for α_i, we get

$$\alpha_i(t) = -\frac{1}{2c_k^2 h_i^{2k+2}} \left(r_h - e_t - (\omega_i)_x, \psi_{k+1,i}\right)_{I_i}. \tag{3.4}$$

Our error estimate procedure consists of approximating the true error on each element I_i as

$$e(x,t) \approx E(x,t) = a_i(t)\psi_{k+1,i}(x), \ x \in I_i,$$

where $a_i(t)$ is an approximation of $\alpha_i(t)$ and is obtained from (3.4) by neglecting the terms involving ω_i and e_t, *i.e.*,

$$a_i(t) = -\frac{1}{2c_k^2 h_i^{2k+2}} \left(r_h, \psi_{k+1,i}\right)_{I_i}. \tag{3.5}$$

We note that $E(x,t) = a_i(t)\psi_{k+1,i}(x), \ x \in I_i$ is a computable quantity since it only depends on the numerical solution u_h and f. Thus, our DG error estimates are computationally simple and are obtained by solving a local steady problems with no boundary conditions on each element.

Next, we will show that the error estimate E converges to the exact error e in the L^2-norm as $h \to 0$. Before stating our main result we state and prove the following preliminary results.

Theorem 3.1. *Suppose that u and u_h respectively, are solutions of (1.1) and (2.2). If α_i and a_i are given by (3.4) and (3.5), then there exists a positive constant C independent of h such that*

$$\sum_{i=1}^{N} (a_i - \alpha_i)^2 \left\|\psi_{k+1,i}\right\|_{I_i}^2 \leq C \ h^{2k+4}. \tag{3.6}$$

$$\sum_{i=1}^{N} (a_i^2 + \alpha_i^2) \left\|\psi_{k+1,i}\right\|_{I_i}^2 \leq C \ h^{2k+2}. \tag{3.7}$$

Proof. Subtracting (3.5) from (3.4), we obtain

$$a_i - \alpha_i = -\frac{1}{2c_k^2 h_i^{2k+2}} (e_t + (\omega_i)_x, \psi_{k+1,i})_{I_i}.$$

Applying the inequality $(a+b)^2 \leq 2(a^2+b^2)$, we obtain

$$\begin{aligned} (a_i - \alpha_i)^2 &= \frac{1}{4c_k^4 h_i^{4k+4}} \left[(e_t + (\omega_i)_x, \psi_{k+1,i})_{I_i}\right]^2 \\ &\leq \frac{1}{2c_k^4 h_i^{4k+4}} \left[(e_t, \psi_{k+1,i})_{I_i}^2 + ((\omega_i)_x, \psi_{k+1,i})_{I_i}^2\right]. \end{aligned}$$

Applying Cauchy-Schwarz inequality, $(x,y)_{I_i}^2 \leq \|x\|_{I_i}^2 \ \|y\|_{I_i}^2$, yields

$$(a_i - \alpha_i)^2 \leq \frac{\|\psi_{k+1,i}\|_{I_i}^2}{2c_k^4 h_i^{4k+4}} \left[\|e_t\|_{I_i}^2 + \|(\omega_i)_x\|_{I_i}^2\right]. \tag{3.8}$$

Multiplying (3.8) by $\|\psi_{k+1,i}\|_{I_i}^2$ and using (2.7) we get

$$\begin{aligned} (a_i - \alpha_i)^2 \left\|\psi_{k+1,i}\right\|_{I_i}^2 &\leq \frac{\|\psi_{k+1,i}\|_{I_i}^4}{2c_k^4 h_i^{4k+4}} \left[\|e_t\|_{I_i}^2 + \|(\omega_i)_x\|_{I_i}^2\right] \\ &= \tilde{c}_k h_i^2 \left[\|e_t\|_{I_i}^2 + \|(\omega_i)_x\|_{I_i}^2\right], \end{aligned} \tag{3.9a}$$

where $\tilde{c}_k$ is a constant given by

$$\tilde{c}_k = \frac{d_k^2}{2c_k^4} = \frac{2(2k+2)^2}{(2k+1)^2(2k+3)^2}. \tag{3.9b}$$

Finally, summing over all elements and use the fact that $h = \max\limits_{1\leq i\leq N} h_i$, we obtain

$$\sum_{i=1}^{N}(a_i-\alpha_i)^2 \left\|\psi_{k+1,i}\right\|_{I_i}^2 \leq \tilde{c}_k h^2 \left[\left\|e_t\right\|^2 + \sum_{i=1}^{N}\left\|(\omega_i)_x\right\|_{I_i}^2\right]. \tag{3.10}$$

Combining this estimate with (2.10c) and (2.12c), with t kept fixed, we establish (3.6).

In order to prove (3.7), we combine (3.1a) and (3.5) to write

$$a_i^2 = \frac{1}{4c_k^4 h_i^{4k+4}} \left(r_h, \psi_{k+1,i}\right)_{I_i}^2 = \frac{1}{4c_k^4 h_i^{4k+4}} \left(e_t + e_x, \psi_{k+1,i}\right)_{I_i}^2. \tag{3.11}$$

Applying the inequality $(a+b)^2 \leq 2(a^2+b^2)$ and Cauchy-Schwarz inequality, we get

$$\begin{aligned} a_i^2 &\leq \frac{1}{2c_k^4 h_i^{4k+4}} \left[\left(e_t, \psi_{k+1,i}\right)_{I_i}^2 + \left(e_x, \psi_{k+1,i}\right)_{I_i}^2\right] \\ &\leq \frac{\left\|\psi_{k+1,i}\right\|_{I_i}^2}{2c_k^4 h_i^{4k+4}} \left[\left\|e_t\right\|_{I_i}^2 + \left\|e_x\right\|_{I_i}^2\right]. \end{aligned} \tag{3.12}$$

Multiplying (3.12) by $\left\|\psi_{k+1,i}\right\|_{I_i}^2$ and using (2.7), we obtain

$$\begin{aligned} a_i^2 \left\|\psi_{k+1,i}\right\|_{I_i}^2 &\leq \frac{\left\|\psi_{k+1,i}\right\|_{I_i}^4}{2c_k^4 h_i^{4k+4}} \left[\left\|e_t\right\|_{I_i}^2 + \left\|e_x\right\|_{I_i}^2\right] \\ &= \tilde{c}_k h_i^2 \left[\left\|e_t\right\|_{I_i}^2 + \left\|e_x\right\|_{I_i}^2\right], \end{aligned} \tag{3.13}$$

where $\tilde{c}_k$ is defined in (3.9b).

Summing over all elements and use the fact that $h = \max\limits_{1\leq i\leq N} h_i$, we write

$$\sum_{i=1}^{N} a_i^2 \left\|\psi_{k+1,i}\right\|_{I_i}^2 \leq \tilde{c}_k h^2 \left[\left\|e_t\right\|^2 + \left\|e\right\|_{1,I}^2\right]. \tag{3.14}$$

By the estimates (2.10c) and (2.13), we obtain

$$\sum_{i=1}^{N} a_i^2 \left\|\psi_{k+1,i}\right\|_{I_i}^2 \leq C h^{2k+2}. \tag{3.15}$$

Taking the L^2 inner product of $\psi_{k+1,i}$ and ϕ_i, defined in (2.8b), and applying Cauchy-Schwarz inequality, we get

$$\left|\alpha_i\right| \left\|\psi_{k+1,i}\right\|_{I_i}^2 = \left|\left(\phi_i, \psi_{k+1,i}\right)_{I_i}\right| \leq \left\|\psi_{k+1,i}\right\|_{I_i} \left\|\phi_i\right\|_{I_i}.$$

Hence, we have

$$\left|\alpha_i\right| \left\|\psi_{k+1,i}\right\|_{I_i} \leq \left\|\phi_i\right\|_{I_i} \quad \Rightarrow \quad \alpha_i^2 \left\|\psi_{k+1,i}\right\|_{I_i}^2 \leq \left\|\phi_i\right\|_{I_i}^2.$$

Summing over all elements and applying (2.8c) we have

$$\sum_{i=1}^{N} \alpha_i^2 \left\|\psi_{k+1,i}\right\|_{I_i}^2 \leq \sum_{i=1}^{N} \left\|\phi_i\right\|_{I_i}^2 \leq C h^{2k+2}. \tag{3.16}$$

Adding (3.15) and (3.16) yields (3.7). □

The main results of this section are stated in the following theorem.

Theorem 3.2. *Assume that the assumptions of Theorem 2.1 are satisfied. If* $a_i,\ i = 1, \cdots, N$, *are given by (3.5) and* $E(x,t) = a_i(t)\psi_{k+1,i}(x),\ x \in\ I_i$, *then there exists a positive constant* C *independent of* h *such that*

$$\|e - E\|^2 \leq C\ h^{2k+4}. \tag{3.17}$$

As a consequence, the DG method combined with the a posteriori error estimation procedure yields $\mathcal{O}(h^{k+2})$ *superconvergent solution i.e.,*

$$\|u - (u_h + E)\|^2 = \sum_{i=1}^{N} \|u - (u_h + a_i\psi_{k+1,i})\|_{I_i}^2 \leq C\ h^{2k+4}. \tag{3.18}$$

Furthermore,

$$\|e\|^2 = \|E\|^2 + \hat{\epsilon} = \sum_{i=1}^{N} a_i^2 \|\psi_{k+1,i}\|_{I_i}^2 + \hat{\epsilon}, \quad \textit{where } |\hat{\epsilon}| \leq C\ h^{2k+3}, \tag{3.19}$$

and as $h \to 0$ *with* t *kept fixed,*

$$\frac{\|E\|}{\|e\|} = 1 + \mathcal{O}(h). \tag{3.20}$$

Proof. First, we will prove (3.17) and (3.18). Since $e = \alpha_i\psi_{k+1,i} + \omega_i$ and $E = a_i\psi_{k+1,i}$ on I_i, we have

$$\|e - E\|_{I_i}^2 = \|(\alpha_i - a_i)\psi_{k+1,i} + \omega_i\|_{I_i}^2 \leq 2(\alpha_i - a_i)^2 \|\psi_{k+1,i}\|_{I_i}^2 + 2\|\omega_i\|_{I_i}^2,$$

where we used the inequality $(a+b)^2 \leq 2a^2 + 2b^2$. Summing over all elements and applying the estimates (2.12c) and (3.6) yields

$$\begin{aligned} \|e - E\|^2 &= \sum_{i=1}^{N} \|e - E\|_{I_i}^2 \leq 2\sum_{i=1}^{N} (\alpha_i - a_i)^2 \|\psi_{k+1,i}\|_{I_i}^2 + 2\sum_{i=1}^{N} \|\omega_i\|_{I_i}^2 \\ &\leq 2C_1 h^{2k+4} + 2C_2 h^{2k+4} = Ch^{2k+4}. \end{aligned}$$

Using the relation $e = u - u_h$ and the estimate (3.17), we obtain

$$\sum_{i=1}^{N} \|u - (u_h + a_i\psi_{k+1,i})\|_{I_i}^2 = \|u - (u_h + E)\|^2 = \|e - E\|^2 \leq Ch^{2k+4}.$$

Next, we will prove (3.19). From (2.15) the DG error can be split as $e = \phi_i + \omega_i,\ on\ \ I_i$. Taking the L^2-norm of the DG error and using (2.8b) we have

$$\|e\|_{I_i}^2 = \|\phi_i\|_{I_i}^2 + 2(\phi_i, \omega_i)_{I_i} + \|\omega_i\|_{I_i}^2 = \alpha_i^2 \|\psi_{k+1,i}\|_{I_i}^2 + \epsilon_i, \tag{3.21a}$$

where

$$\epsilon_i = 2(\phi_i, \omega_i)_{I_i} + \|\omega_i\|_{I_i}^2. \tag{3.21b}$$

Summing over all elements, we obtain

$$\|e\|^2 = \sum_{i=1}^{N} \alpha_i^2 \|\psi_{k+1,i}\|_{I_i}^2 + \tilde{\epsilon}, \quad \text{where} \quad \tilde{\epsilon} = \sum_{i=1}^{N} \epsilon_i. \tag{3.22}$$

Next, we write the DG error as

$$\|e\|^2 = \sum_{i=1}^{N} a_i^2 \left\|\psi_{k+1,i}\right\|_{I_i}^2 + \hat{\epsilon}, \text{ where } \hat{\epsilon} = \sum_{i=1}^{N} (\alpha_i^2 - a_i^2) \left\|\psi_{k+1,i}\right\|_{I_i}^2 + \tilde{\epsilon}. \tag{3.23}$$

From (3.21b), we apply Cauchy-Schwarz inequality to obtain

$$|\epsilon_i| \leq 2 \left\|\phi_i\right\|_{I_i} \left\|\omega_i\right\|_{I_i} + \left\|\omega_i\right\|_{I_i}^2. \tag{3.24}$$

Summing over all elements and applying the Cauchy-Schwarz inequality with the estimates (2.8c) and (2.12c), we get

$$|\tilde{\epsilon}| \leq \sum_{i=1}^{N} |\epsilon_i| \leq C_1 \ h^{2k+3}. \tag{3.25}$$

Next, we bound the first term in $\hat{\epsilon}$ using Cauchy-Schwarz inequality and the inequality $(a+b)^2 \leq 2a^2 + 2b^2$ as

$$\begin{aligned}
&\sum_{i=1}^{N} (\alpha_i^2 - a_i^2) \left\|\psi_{k+1,i}\right\|_{I_i}^2 \\
= \ &\sum_{i=1}^{N} \Big((\alpha_i - a_i) \left\|\psi_{k+1,i}\right\|_{I_i} \Big) \Big((\alpha_i + a_i) \left\|\psi_{k+1,i}\right\|_{I_i} \Big) \\
\leq \ &\left(\sum_{i=1}^{N} (\alpha_i - a_i)^2 \left\|\psi_{k+1,i}\right\|_{I_i}^2 \right)^{1/2} \left(\sum_{i=1}^{N} (\alpha_i + a_i)^2 \left\|\psi_{k+1,i}\right\|_{I_i}^2 \right)^{1/2} \\
\leq \ &\sqrt{2} \left(\sum_{i=1}^{N} (\alpha_i - a_i)^2 \left\|\psi_{k+1,i}\right\|_{I_i}^2 \right)^{1/2} \left(\sum_{i=1}^{N} (\alpha_i^2 + a_i^2) \left\|\psi_{k+1,i}\right\|_{I_i}^2 \right)^{1/2}.
\end{aligned}$$

Applying the estimates (3.6) and (3.7), we get

$$\sum_{i=1}^{N} (\alpha_i^2 - a_i^2) \left\|\psi_{k+1,i}\right\|_{I_i}^2 \leq C_1 \ h^{2k+3}. \tag{3.26}$$

Finally, combining (3.23), (3.25) and (3.26) completes the proof of (3.19).

In order to prove (3.20) we use (3.19) to write

$$\|e\|^2 = \|E\|^2 + \hat{\epsilon}. \tag{3.27}$$

Dividing by $\|e\|^2$ and using the fact that $\|e\|^2 = \mathcal{O}(h^{2k+2})$ and $\hat{\epsilon} = \mathcal{O}(h^{2k+3}) = K \ h^{2k+3}$, for some constant K, we obtain

$$\frac{\|E\|^2}{\|e\|^2} = 1 - K \ h,$$

which, after taking the square root and using the Maclaurin series with respect to h of $(1 - K \ h)^{1/2} = 1 - \frac{K}{2}h + \cdots = 1 + \mathcal{O}(h)$, completes the proof of (3.20). □

An accepted efficiency measure of *a posteriori* error estimate is the global effectivity index defined as follows:

$$\theta(t) = \frac{\|E\|}{\|e\|}.$$

Ideally, the global effectivity index should stay close to one and should converge to one under mesh refinement.

In the previous theorem, we proved that the global *a posteriori* error estimates at a fixed time t converge to the true spatial errors at $\mathcal{O}(h^{k+2})$ rate. We further proved that the global effectivity index in the L^2-norm converges to unity at $\mathcal{O}(h)$ rate. We note that the computable quantity $u_h + E$ converge to the exact solution u at $\mathcal{O}(h^{k+2})$ rate. We emphasize that this accuracy enhancement is achieved by adding the error estimate E to the approximate solution u_h only once at the end of the computation *i.e.*, at $t = T$. This leads to very efficient computations of the post-processed approximation $u_h + E$. Additionally, it is computationally efficient because our DG error estimates are obtained by solving a local steady problem with no boundary conditions on each element.

4. Numerical examples

In this section, we present several numerical examples to demonstrate the global convergence of the residual-based *a posteriori* error estimates. The initial condition is determined by $u_h(x,0) = P_h^- u(x,0),\ x \in I_i,\ i = 1, \cdots, N$. Even though Theorem 2.1 requires the initial condition designed in [32], we have observed similar results if we use the projection P_h^- and the standard L^2 projection of the initial condition instead. See the numerical experiments in [32] for some discussion related to initial conditions for conservation laws. Temporal integration is performed by the fourth-order classical explicit Runge-Kutta method. A time step Δt is chosen so that temporal errors are small relative to spatial errors.

Let δe and $\delta\theta$ be defined as

$$\delta e(t) = \big|\, \|e\| - \|E\| \,\big|, \quad \delta\theta(t) = \big|\theta(t) - 1\big|, \quad \text{where} \quad \theta(t) = \frac{\|E\|}{\|e\|}.$$

Example 4.1. *We consider the following initial-boundary value problem*

$$\begin{cases} u_t + u_x = 0, \quad x \in [-1,1],\ t \in [0,1], \\ u(x,0) = \sin(\pi x), \quad x \in [-1,1], \\ u(-1,t) = \sin(\pi t), \quad t \in [0,1]. \end{cases}$$

The exact solution is given by $u(x,t) = \sin(\pi(x-t))$. We solve this problem using the DG method on uniform meshes obtained by partitioning the domain $[-1,1]$ into N subintervals with $N = 5$, 10, 20, 30, 40, 50 and using the spaces P^k with $k = 1-3$. In Figure 1 we plot, in log-log scale, the L^2 errors $||e||$ at time $t = 1$ versus h. For each P^k space, we fit, in a least-squares sense, the data sets with a linear function and then calculate from the fitting result the slopes of the fitting lines. The slopes of the fitting lines are shown on the graph. We observe that $||e|| = \mathcal{O}(h^{k+1})$.

On each element, we apply the error estimation procedure (3.5) to compute the error estimates for the DG solution. In Figure 1, we present the convergence rates for the global errors $||e-E||$ using the spaces P^k with $k = 1-3$. These results indicate that $||e - E|| = \mathcal{O}(h^{k+2})$. This is in full agreement with the theory. This example demonstrates that the superconvergence rate proved in this paper is optimal. We note that

$$||e - E|| = ||u - u_h - E|| = ||u - (u_h + E)|| = \mathcal{O}(h^{k+2}).$$

Thus, the computable quantities $u_h + E$ converge to the exact solution u at $\mathcal{O}(h^{k+2})$ rate. We note that this accuracy enhancement is achieved by adding the error

estimate E to the DG solution only once at the end of the computation *i.e.*, at $t = T$. This leads to a very efficient computation of the post-processed approximation $u_h + E$. Also, we note that $u_h + E$ is computationally efficient because our DG error estimate E, $x \in I_i$ is obtained by solving a local steady problem with no boundary conditions on each element.

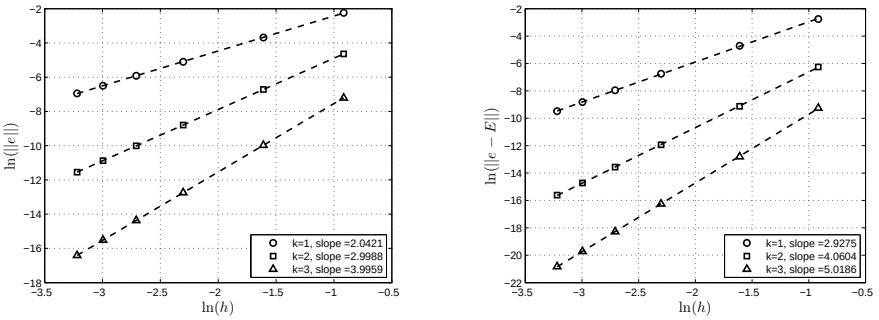

Figure 1: Convergence rates at $t = 1$ for $||e||$ (left) and $||e - E||$ (right) for Example 4.1 on uniform meshes having $N = 5$, 10, 20, 30, 40, 50 elements using P^k, $k = 1$ to 3. The slopes of the fitting lines are shown on the graph.

The true L^2 errors and the global effectivity indices shown in Table 1 indicate that our *a posteriori* error estimates converge to the true errors under both h- and p-refinements. The results shown in Figure 2 indicate that the numerical convergence

TABLE 1. L^2 errors and global effectivity indices for Example 4.1 on uniform meshes having N =5, 10, 20, 30, 40, 50 elements using P^k, $k = 1$ to 3.

N	$k=1$		$k=2$		$k=3$	
	$\|\|e\|\|$	θ	$\|\|e\|\|$	θ	$\|\|e\|\|$	θ
5	1.0653e-1	0.7897	9.6525e-3	0.9545	7.4001e-4	0.9792
10	2.5073e-2	0.9302	1.2096e-3	0.9888	4.6654e-5	0.9939
20	6.0850e-3	0.9806	1.5126e-4	0.9972	2.9201e-6	0.9987
30	2.6859e-3	0.9912	4.4824e-5	0.9988	5.7701e-7	0.9994
40	1.5069e-3	0.9950	1.8911e-5	0.9993	1.8259e-7	0.9997
50	9.6322e-4	0.9968	9.6826e-6	0.9996	7.4795e-8	0.9998

rate at $t = 1$ for δe is $\mathcal{O}(h^{k+3})$. The observed rate is higher than the theoretical rate which is proved to be of order $k+3/2$. The errors $\delta\theta$ and their orders of convergence shown in Figure 2 suggest that the convergence rate at $t = 1$ for $\delta\theta$ is $\mathcal{O}(h^2)$ under mesh refinement. These results indicate that the observed numerical convergence rate is higher than the theoretical rate established in Theorem 3.2 which is proved to be of order $\mathcal{O}(h)$. We note that the effectivity indices stay close to unity for all times as shown in Figure 3 and converge under h- and $p-$refinements. Numerical results further indicate that the error estimates converge to the true errors with decreasing mesh size and increasing polynomial degree k.

Example 4.2. *In this example, we test the global convergence of our error estimates using nonuniform meshes. We repeat the problem in example 4.1 with all*

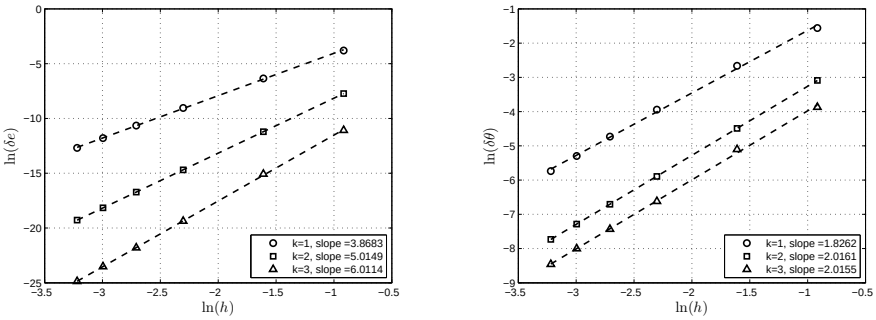

Figure 2: Convergence rates at $t = 1$ for δe (left) and $\delta\theta$ (right) for example 4.1 on uniform meshes having $N = 5$, 10, 20, 30, 40, 50 elements using P^k, $k = 1$ to 3. The slopes of the fitting lines are shown on the graph.

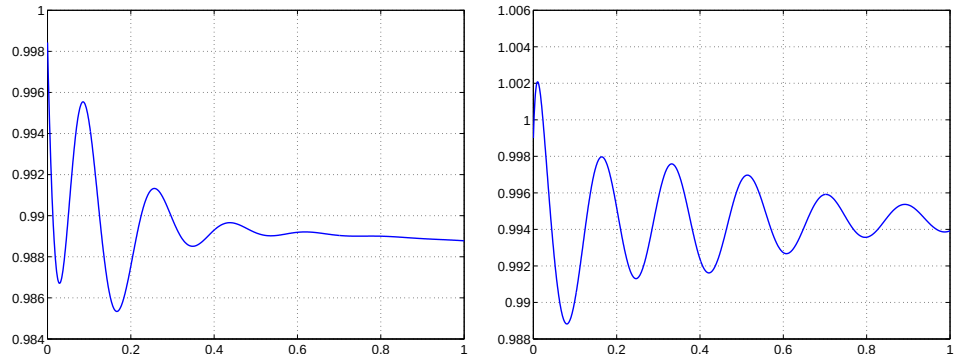

Figure 3: Global effectivity index $\theta(t)$ versus time for Example 4.1 on uniform meshes having $N = 10$ elements using P^2 (left) and P^3 (right).

parameters kept unchanged except for meshes where we consider nonuniform meshes constructed as follows: First, we partition the entire domain $[-1, 1]$ *into nodes* $-1 = x_0 < x_1 < \cdots < x_{\frac{N}{3}} = 1$ *with* $N = 12$, *18, 24, 30, 36, 42 to form* $\frac{N}{3}$ *subintervals, where* N *is a multiple of three, each of length* $h_0 = \frac{6}{N}$. *Each subinterval is then divided into three nonuniform subintervals of length* $\frac{h_0}{7}$, $\frac{h_0}{2}$, *and* $\frac{5h_0}{14}$, *respectively.*

The L^2 errors as well as their order of convergence at $t = 1$ are shown in Figure 4. These results show the DG method yields $\mathcal{O}(h^{k+1})$ convergent solution. The L^2 DG errors $||e-E||$ at time $t = 1$ shown in Figure 4 suggest optimal $\mathcal{O}(h^{k+2})$ convergence rate. Next, we present the true L^2 errors and the global effectivity indices in Table 2. We observe that the error estimates converge to the true errors in the L^2-norm under both h- and p-refinements. The results shown in Figure 5 indicate that the numerical convergence rate at $t = 1$ for δe is $\mathcal{O}(h^{k+3})$. The observed rate is again higher than the theoretical rate which is proved to be of order $k+3/2$. The errors $\delta\theta$ and their orders of convergence shown in Figure 5 suggest that the global effectivity indices converge to the true errors under h- and p-refinements. The convergence rate at $t = 1$ for $\delta\theta$ is $\mathcal{O}(h^2)$. Again, the observed numerical convergence rate is higher than the theoretical rate established in Theorem 3.2.

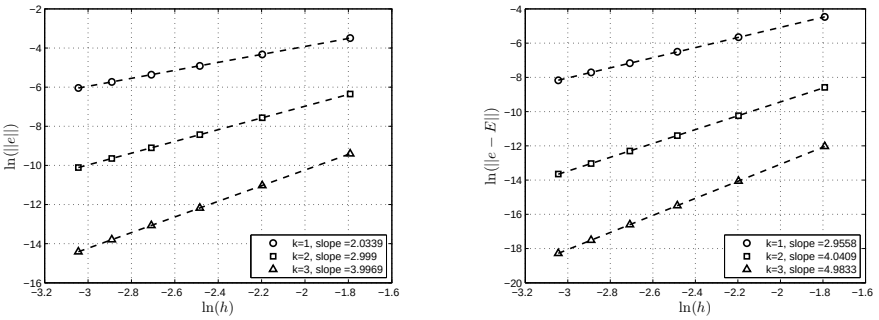

Figure 4: Convergence rates at $t = 1$ for $||e||$ (left) and $||e - E||$ (right) for example 4.2 on nonuniform meshes having $N = 12$, 18, 24, 30, 36, 42 elements using P^k, $k = 1$ to 3. The slopes of the fitting lines are shown on the graph.

TABLE 2. L^2 errors and global effectivity indices for Example 4.2 on nonuniform meshes having $N = 12$, 18, 24, 30, 36, 42 elements using P^k, $k = 1$ to 3.

N	$k=1$		$k=2$		$k=3$	
	$\|\|e\|\|$	θ	$\|\|e\|\|$	θ	$\|\|e\|\|$	θ
12	3.0371e-2	0.9132	1.7468e-3	0.9841	8.2279e-5	0.9918
18	1.3192e-2	0.9580	5.1784e-4	0.9931	1.6295e-5	0.9962
24	7.3448e-3	0.9757	2.1855e-4	0.9961	5.1601e-6	0.9978
30	4.6763e-3	0.9842	1.1192e-4	0.9975	2.1143e-6	0.9986
36	3.2378e-3	0.9890	6.4773e-5	0.9982	1.0198e-6	0.9991
42	2.3744e-3	0.9918	4.0793e-5	0.9987	5.5052e-7	0.9993

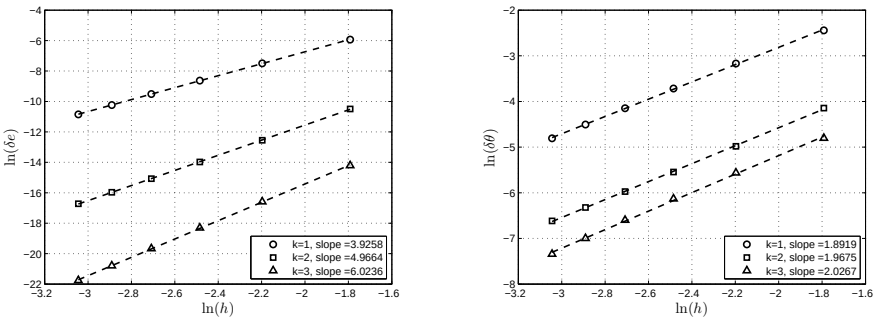

Figure 5: Convergence rates at $t = 1$ for δe (left) and $\delta\theta$ (right) for example 4.2 on nonuniform meshes having $N = 12$, 18, 24, 30, 36, 42 elements using P^k, $k = 1$ to 3. The slopes of the fitting lines are shown on the graph.

Example 4.3. *In this example, we demonstrate that our results hold true when using periodic boundary condition (1.1d) instead of (1.1c). For this, we solve the following problem*

$$\begin{cases} u_t + u_x = 0, \quad x \in [-1, 1], \ t \in [0, 1], \\ u(x, 0) = \sin(\pi x), \quad x \in [-1, 1], \end{cases}$$

with periodic boundary condition $u(-1, t) = u(1, t)$. *The exact solution to this problem is* $u(x, t) = \sin(\pi(x - t))$.

We solve this problem using the DG method on uniform meshes having $N = 5$, 10, 20, 30, 40, 50 elements and using the spaces P^k with $k = 1,\ 2$ and 3. We present the true errors in Figure 6 at time $t = 1$. These results indicate that $||e|| = \mathcal{O}(h^{k+1})$, where $h = \max\limits_{1\le i\le N} h_i$. The L^2 DG errors $||e - E||$ at time $t = 1$ shown in Figure 6 suggest optimal $\mathcal{O}(h^{k+2})$ convergence rate. The results presented in Table 3 indicate that the global effectivity indices converge to the true errors under mesh refinement. The results shown in Figure 7 indicate that the numerical convergence rate at $t = 1$ for δe is $\mathcal{O}(h^{k+3})$. Finally, the errors $\delta\theta$ and their orders of convergence shown in Figure 7 suggest that the global effectivity indices converge to the true errors under h-refinement. The convergence rate at $t = 1$ for $\delta\theta$ is $\mathcal{O}(h^2)$ under mesh refinement. Again the observed numerical convergence rates for δe and $\delta\theta$ are higher than the theoretical rates which are proved to be $\mathcal{O}(h^{k+3/2})$ and $\mathcal{O}(h)$, respectively. We conclude that our results for uniform meshes also hold true for this random mesh. We have also used a random mesh which is a random perturbation of the uniform mesh and observed similar results. These numerical results, which are not included to save space, still show the same rates of convergence for $||e-E||$, δe, and $\delta\theta$.

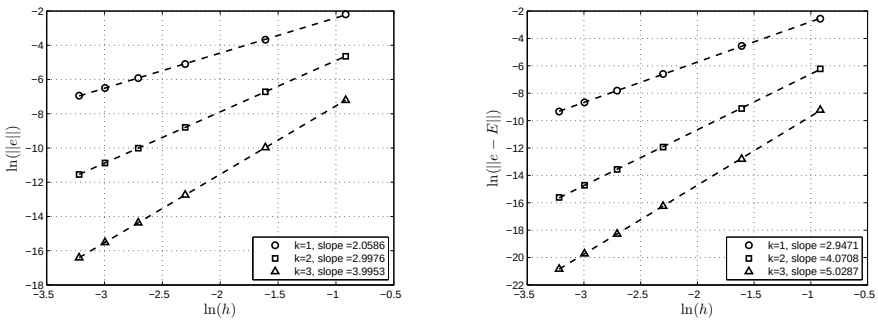

Figure 6: Convergence rates at $t = 1$ for $||e||$ (left) and $||e - E||$ (right) at time $t = 1$ versus mesh sizes h for Example 4.3 on uniform meshes having $N = 5$, 10, 20, 30, 40, 50 elements using P^k, $k = 1$ to 3. The slopes of the fitting lines are shown on the graph.

TABLE 3. L^2 errors and global effectivity indices for Example 4.3 on uniform meshes having $N = 5$, 10, 20, 30, 40, 50 elements using P^k, $k = 1$ to 3.

N	$k=1$		$k=2$		$k=3$	
	$\|\|e\|\|$	θ	$\|\|e\|\|$	θ	$\|\|e\|\|$	θ
5	1.1115e-1	0.7491	9.6203e-3	0.9564	7.3828e-4	0.9834
10	2.5330e-2	0.9199	1.2093e-3	0.9890	4.6707e-5	0.9929
20	6.1006e-3	0.9780	1.5126e-4	0.9973	2.9201e-6	0.9988
30	2.6889e-3	0.9900	4.4824e-5	0.9988	5.7701e-7	0.9994
40	1.5079e-3	0.9943	1.8911e-5	0.9993	1.8259e-7	0.9997
50	9.6363e-4	0.9963	9.6825e-6	0.9996	7.4795e-8	0.9998

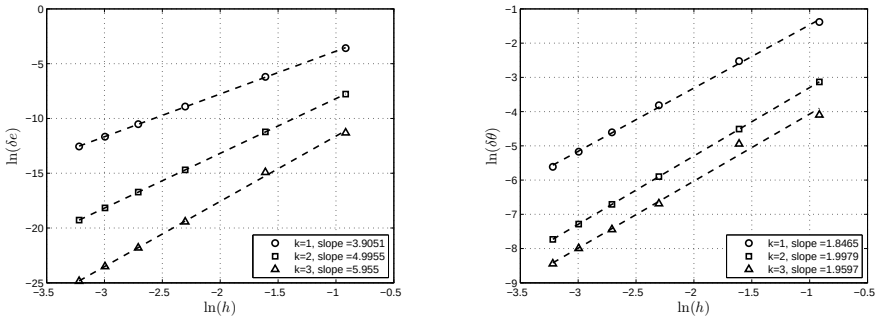

Figure 7: Convergence rates at $t = 1$ for δe (left) and $\delta\theta$ (right) for example 4.3 on uniform meshes having $N = 5$, 10, 20, 30, 40, 50 elements using P^k, $k = 1$ to 3. The slope of the fitting line is indicated on the top of each figure.

5. Concluding remarks

In this paper we analyzed the global convergence of the implicit residual-based *a posteriori* error estimates for the DG method applied to one-dimensional linear hyperbolic problems. We used a new optimal superconvergence result [32] to prove that these *a posteriori* error estimates converge to the true spatial errors at $\mathcal{O}(h^{k+2})$ rate. We also proved that the global effectivity indices in the L^2-norm converge to unity at $\mathcal{O}(h)$ rate. These results improve upon our previously published work in which the orders of convergence for the *a posteriori* error estimates and the global effectivity indices are proved to be $k + 3/2$ and $1/2$, respectively. Furthermore, we proved that the DG method combined with the *a posteriori* error estimation procedure yields both accurate error estimates and $\mathcal{O}(h^{k+2})$ superconvergent solutions. Our proofs are valid for arbitrary regular meshes, for P^k polynomials with $k \geq 1$, and for both the periodic boundary condition and the initial-boundary value problem. We are currently investigating the superconvergence properties of the local DG method applied to two-dimensional convection-diffusion problems and two-dimensional wave equations on rectangular and triangular meshes. Superconvergence on more general meshes and nonlinear problems will be investigated in the future.

Acknowledgments

The author would also like to thank the anonymous referees for their constructive comments and remarks which helped improve the quality and readability of the paper. This research was partially supported by the NASA Nebraska Space Grant Program and UCRCA at the University of Nebraska at Omaha.

References

[1] M. Abramowitz, I. A. Stegun, Handbook of Mathematical Functions, Dover, New York, 1965.
[2] S. Adjerid, M. Baccouch, The discontinuous Galerkin method for two-dimensional hyperbolic problems. I: Superconvergence error analysis, Journal of Scientific Computing 33 (2007) 75–113.
[3] S. Adjerid, M. Baccouch, The discontinuous Galerkin method for two-dimensional hyperbolic problems. II: *A posteriori* error estimation, Journal of Scientifc Computing 38 (2009) 15–49.

[4] S. Adjerid, M. Baccouch, Asymptotically exact a posteriori error estimates for a one-dimensional linear hyperbolic problem, Applied Numerical Mathematics 60 (2010) 903–914.
[5] S. Adjerid, K. D. Devine, J. E. Flaherty, L. Krivodonova, A posteriori error estimation for discontinuous Galerkin solutions of hyperbolic problems, Computer Methods in Applied Mechanics and Engineering 191 (2002) 1097–1112.
[6] S. Adjerid, A. Klauser, Superconvergence of discontinuous finite element solutions for transient convection-diffusion problems, Journal of Scientific computing 22 (2005) 5–24.
[7] S. Adjerid, T. C. Massey, A posteriori discontinuous finite element error estimation for two-dimensional hyperbolic problems, Computer Methods in Applied Mechanics and Engineering 191 (2002) 5877–5897.
[8] S. Adjerid, H. Temimi, A discontinuous Galerkin method for higher-order ordinary differential equations, Computer Methods in Applied Mechanics and Engineering 197 (2007) 202–218.
[9] M. Ainsworth, J. T. Oden, A posteriori Error Estimation in Finite Element Analysis, John Wiley, New York, 2000.
[10] M. Baccouch, A local discontinuous Galerkin method for the second-order wave equation, Computer Methods in Applied Mechanics and Engineering 209–212 (2012) 129–143.
[11] M. Baccouch, S. Adjerid, Discontinuous Galerkin error estimation for hyperbolic problems on unstructured triangular meshes, Computer Methods in Applied Mechanics and Engineering 200 (2010) 162–177.
[12] F. Bassi, S. Rebay, A high-order accurate discontinuous finite element method for the numerical solution of the compressible Navier-Stokes equations, Journal of Computational Physics 131 (1997) 267–279.
[13] C. E. Baumann, J. T. Oden, A discontinuous hp finite element method for convection-diffusion problems, Computer Methods in Applied Mechanics and Engineering 175 (1999) 311–341.
[14] K. S. Bey, J. T. Oden, hp-version discontinuous Galerkin method for hyperbolic conservation laws, Computer Methods in Applied Mechanics and Engineering 133 (1996) 259–286.
[15] K. S. Bey, J. T. Oden, A. Patra, hp-version discontinuous Galerkin method for hyperbolic conservation laws: A parallel strategy, International Journal of Numerical Methods in Engineering 38 (1995) 3889–3908.
[16] K. S. Bey, J. T. Oden, A. Patra, A parallel hp-adaptive discontinuous Galerkin method for hyperbolic conservation laws, Applied Numerical Mathematics 20 (1996) 321–386.
[17] R. Biswas, K. Devine, J. E. Flaherty, Parallel adaptive finite element methods for conservation laws, Applied Numerical Mathematics 14 (1994) 255–284.
[18] K. Bottcher, R. Rannacher, Adaptive error control in solving ordinary differential equations by the discontinuous Galerkin method, Tech. report, University of Heidelberg (1996).
[19] P. Castillo, A superconvergence result for discontinuous Galerkin methods applied to elliptic problems, Computer Methods in Applied Mechanics and Engineering 192 (2003) 4675–4685.
[20] F. Celiker, B. Cockburn, Superconvergence of the numerical traces for discontinuous Galerkin and hybridized methods for convection-diffusion problems in one space dimension, Mathematics of Computation 76 (2007) 67–96.
[21] Y. Cheng, C.-W. Shu, Superconvergence of discontinuous Galerkin and local discontinuous Galerkin schemes for linear hyperbolic and convection-diffusion equations in one space dimension, SIAM Journal on Numerical Analysis 47 (2010) 4044–4072.
[22] B. Cockburn, G. E. Karniadakis, C. W. Shu, Discontinuous Galerkin Methods Theory, Computation and Applications, Lecture Notes in Computational Science and Engineering, vol. 11, Springer, Berlin, 2000.
[23] B. Cockburn, S. Y. Lin, C. W. Shu, TVB Runge-Kutta local projection discontinuous Galerkin methods of scalar conservation laws III: One dimensional systems, Journal of Computational Physics 84 (1989) 90–113.
[24] B. Cockburn, C. W. Shu, TVB Runge-Kutta local projection discontinuous Galerkin methods for scalar conservation laws II: General framework, Mathematics of Computation 52 (1989) 411–435.
[25] M. Delfour, W. Hager, F. Trochu, Discontinuous Galerkin methods for ordinary differential equation, Mathematics of Computation 154 (1981) 455–473.
[26] K. D. Devine, J. E. Flaherty, Parallel adaptive hp-refinement techniques for conservation laws, Computer Methods in Applied Mechanics and Engineering 20 (1996) 367–386.
[27] J. E. Flaherty, R. Loy, M. S. Shephard, B. K. Szymanski, J. D. Teresco, L. H. Ziantz, Adaptive local refinement with octree load-balancing for the parallel solution of three-dimensional conservation laws, Journal of Parallel and Distributed Computing 47 139–152.

[28] C. Johnson, Error estimates and adaptive time-step control for a class of one-step methods for stiff ordinary differential equations, SIAM Journal on Numerical Analysis 25 (1988) 908–926.
[29] P. Lesaint, P. Raviart, On a finite element method for solving the neutron transport equations, in: C. de Boor (ed.), Mathematical Aspects of Finite Elements in Partial Differential Equations, Academic Press, New York, 1974.
[30] W. H. Reed, T. R. Hill, Triangular mesh methods for the neutron transport equation, Tech. Rep. LA-UR-73-479, Los Alamos Scientific Laboratory, Los Alamos (1973).
[31] M. F. Wheeler, An elliptic collocation-finite element method with interior penalties, SIAM Journal on Numerical Analysis 15 (1978) 152–161.
[32] Y. Yang, C.-W. Shu, Analysis of optimal superconvergence of discontinuous Galerkin method for linear hyperbolic equations, SIAM Journal on Numerical Analysis 50 (2012) 3110–3133.

Department of Mathematics, University of Nebraska at Omaha, Omaha, NE 68182, USA

E-mail: mbaccouch@unomaha.edu

URL: http://myweb.unomaha.edu/∼mbaccouch/